Materials Research Express

PAPER

n-type In_2S_3 films deposited by pulsed laser deposition: effect of laser power on the properties of the films

Chunyan Wu, Dun Mao, Zhu Liu, Qi Liang, Shirong Chen, Yongqiang Yu, Li Wang, Linbao Luo and Jun Xu

School of Electronic Science and Applied Physics, Hefei University of Technology, Hefei Anhui 230009, People's Republic of China

E-mail: cywu@hfut.edu.cn **and** luolb@hfut.edu.cn

Keywords: In_2S_3 film, pulsed laser deposition, photovoltaic devices

RECEIVED
16 December 2014

REVISED
27 February 2015

ACCEPTED FOR PUBLICATION
17 April 2015

PUBLISHED
19 May 2015

Abstract

Pulsed laser deposition (PLD) with different levels of laser power was first used to deposit In_2S_3 films from homemade, high-purity In_2S_3 targets. This process was followed by post-annealing in an N_2 atmosphere to improve the films' crystallinity and conductivity. The annealed films were verified to be stoichiometric, body-centered, tetragonal In_2S_3 with the preferred orientation (103). The bandgap of the films decreased from 2.8 to 2.2 eV with an increase in the laser power, which was believed to be the result of the grain growth caused by the higher laser power. The electrical transport property of the bottom-gate field-effect transistor revealed the n-type conduction of the annealed In_2S_3 films, and the heterojunction p^+-Si/annealed In_2S_3 film showed remarkable photovoltaic behavior upon light illumination, indicating that PLD-deposited In_2S_3 films may have great potential as a buffer layer in thin-film solar cells. What's more, doped In_2S_3 films can be easily realized due to the fairly stoichiometric transfer of the PLD method.

1. Introduction

Indium sulfide (In_2S_3), one of the important III–VI group semiconductor compounds, is known to exist in three different crystalline forms: α-In_2S_3 (defect cubic), β-In_2S_3 (defect spinel), and γ-In_2S_3 (layered structure) [1]. Among these, β-In_2S_3 is the stable form at room temperature, and it exists in either a cubic or tetragonal crystal structure [2], or as an n-type semiconductor with a direct bandgap of 2.0–2.3 eV and a high optical transmittance (70–80%) in the visible region [3]. What's more, the intrinsic vacant sites in the lattice that arise from the defect spinel structure of β-In_2S_3 exhibit electron affinity and can act as electron traps [4], which paves the way for optoelectronic device-based applications such as photocatalysis [5, 6], photodetectors [7], and solar cells [8, 9]. Most interestingly, β-In_2S_3 was recently reported to be a promising buffer layer for environmentally friendly solar cells, due to the fact that solar-cell devices prepared using β-In_2S_3 as the buffer layer showed a comparable conversion efficiency to that of the standard CdS buffer layer [10, 11].

Much effort has been made to synthesize β-In2S3 thin films for solar-cell applications. Compared to other deposition techniques for β-In_2S_3 thin films, such as chemical bath deposition [3], spray pyrolysis [12], single-source organometallic chemical vapor deposition [13], and atomic layer deposition [14], the physical vapor deposition (PVD) technique has immense potential to meet the requirements for the industrial production of large-area solar cells and modules [11, 15]. However, the thermal evaporated layers are generally nonstoichiometric, which may limit the solar cells' performance. To address the issue of nonstoichiometry in the evaporated layer, the flash evaporation technique was developed, and a conversion efficiency of 12.6% was delivered by a high flash-rate In2S3 buffered cell [16].

The pulsed laser deposition (PLD) technique is another kind of important PVD technique that is known to be able to render the fairly stoichiometric transfer of atomic species from a bulk target to a thin film under controlled ambient conditions for a diverse class of systems, especially those with complex stoichiometric proportions [17–19]. The properties of the obtained thin films can be tuned on process variables such as laser power, deposition temperature, ambient atmosphere, ambient pressure, etc. Doping can also be easily realized by incorporating the dopant into the bulk target. However, to the best of our knowledge, the synthesis of In_2S_3

films by PLD has received little attention. Herein, we report the deposition of pure stoichiometric In_2S_3 films on Si, SiO_2, and glass for evaluation of their electronic and photovoltaic properties. A remarkable photovoltaic behavior can be observed on the p^+-Si/In_2S_3 heterojunction, which indicates that PLD-deposited In_2S_3 films may have great potential as the buffer layer in thin-film solar cells.

2. Experimental details

8 g of In_2S_3 powder (Alfa Aesar, purity 99.98%) filtered through a 2000-mesh filter was put into a stainless steel mold with a diameter of 25 mm. The mold was pressed with pressures of 10 and 20 MPa for 15 min each, and then maintained at 40 MPa for 4 h by a pressing machine (MTI Corporation, 11 t). The obtained In_2S_3 target was calcined in a programmed horizontal tube furnace in an Ar atmosphere that was heated to 300 °C at a rate of 15 °C min^{-1} and held at this temperature for 2 h. The target was then heated to 750 °C at a rate of 15 °C min^{-1} and maintained at this temperature for 5 h.

The homemade In_2S_3 target was mounted on the target holder of the PLD system. Different kinds of substrates, glass slides, p^+-Si, and SiO_2 (300 nm)/p^+-Si with the size 1 cm × 1 cm were used for the deposition of In_2S_3 films after being successively cleaned with acetone, alcohol, and deionized water. Dark reddish-brown films were obtained after a 30 min deposition in the PLD system by ablating the homemade In_2S_3 target with a KrF excimer laser (Lambda Physik COMPexPro 102, laser wavelength 248 nm, pulse width 25 ns, and frequency 5 Hz). Different laser powers of 87, 138, and 174 mJ were used, and the obtained films were marked as IS1, IS2, and IS3, respectively. After deposition, the films were annealed in a rapid annealing furnace at 350 °C for 5 min in an N_2 atmosphere.

The obtained thin films were characterized by x-ray diffraction (XRD, Rigaku D/Max-γB, with Cu Kα radiation), field-emission scanning electron microscopy (FEI Sirion 200) and atom force microscopy (AFM, CSPM 4000). Compositions of the products were detected by energy-dispersive x-ray spectroscopy (EDS, Oxford INCA, attached to scanning electron microscopy (SEM)). Ultraviolet-visible (UV–vis) absorption spectra were performed on a UV–vis spectrometer (CARY 5000).

To assess the electrical properties of the In_2S_3 films, bottom-gate field-effect transistors (FETs) based on the In_2S_3 films were constructed. In (50 nm) electrodes were deposited by thermal evaporation onto the In_2S_3 films grown in SiO_2 (300 nm)/p^+-Si through a shadow mask. The heavily doped Si substrate acted as the global bottom gate in the nanoFETs. To construct the p^+-Si/In_2S_3 heterojunction, a strip of cellotape was stuck at one edge of the p^+-Si substrate before the In_2S_3 film was deposited. In (50 nm) electrodes were deposited onto the In_2S_3 films and Ag paste contacts were formed at the edge of the p^+-Si substrate after removing the cellotape. All the electrical characterizations were conducted on a semiconductor characterization system (Keithley 4200-SCS), and white light from the optical microscopy on the probe station (2.6 mW cm^{-2}) was used as the light source to detect the photovoltaic characteristics.

3. Results and discussion

Since the as-deposited In_2S_3 films proved to have poor crystallinity, and better crystallinity without obvious stoichiometric deviation can be obtained after annealing at 300–400 °C [20], we chose to post-anneal all the as-deposited In_2S_3 films in an N_2 atmosphere at 350 °C for 5 min. Figure 1(a) shows the XRD patterns of the as-deposited and annealed IS3 films grown on the Si (001) surface. A remarkable amorphous broadening can be observed in the as-deposited film, verifying the poor crystallinity. However, the obvious diffraction peak at 44.5° can be indexed to the crystal plane (309) of the body-centered tetragonal In_2S_3 (JCPDS No. 73-1366), which shows the preferred orientation (103) of the In_2S_3 film. The degree of crystallinity was greatly improved after annealing and the preferred orientation (103) still remained. Although heating the substrate (200–350 °C) has been proven to improve the crystallinity of the In_2S_3 films grown by spray pyrolysis [12] and evaporation methods [20], it has no remarkable effect on PLD-deposited In_2S_3 films. The reason may be that the grains initiated by laser in the PLD system have much higher energy when compared to other methods, which is more beneficial to the crystallization of the as-deposited In_2S_3 films than the substrate temperature. The SEM image in figure 1(b) was taken from the cross section of the annealed IS3 film, which gives a relatively smooth surface and a thickness of about 350 nm. The corresponding EDS spectrum, seen in the inset in figure 1(b), gives the In:S atomic ratio of 4.32:6.56, which is very close to the stoichiometric ratio of In_2S_3. Therefore, we can see that a fairly stoichiometric transfer from the homemade In_2S_3 target to the tetragonal In_2S_3 films has been realized. XRD patterns and EDS spectra of the other In_2S_3 films give similar results, which are not shown here.

In_2S_3 films grown on glass substrates were annealed and used for the UV–vis absorption, and the corresponding spectra are described in figure 2. It can be observed that all the films showed a similar absorbance when the incident wavelength was larger than ~600 nm. However, when the incident wavelength was smaller

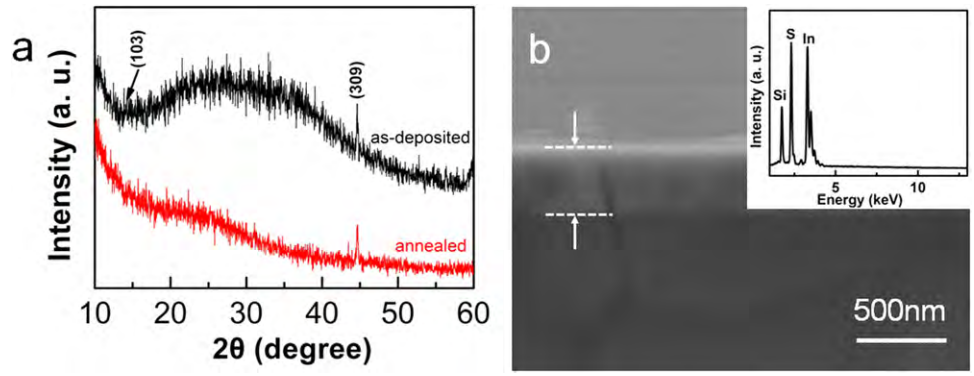

Figure 1. (a) XRD patterns of the as-deposited and annealed IS3 films grown on an Si (001) surface. (b) SEM image taken from the cross section of the annealed IS3 film. Inset shows the corresponding EDS spectrum.

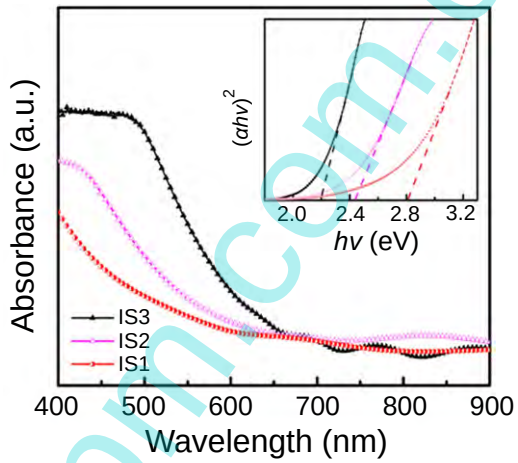

Figure 2. UV–vis absorption spectra of the annealed In_2S_3 films grown on glass substrates. Inset shows the corresponding $(\alpha h\upsilon)^2$–$h\upsilon$ plots.

than ~600 nm, the absorbance of the films increased from IS1 to IS3, which may be attributed to the different optical energy bandgaps of the films.

The optical energy bandgap (E_g) of the annealed In_2S_3 films can be deduced using the equation

$$ah\upsilon = \mathrm{A}\left(h\upsilon - E_g\right)^n$$

where A is an energy-independent constant. n is an exponent that is determined by the type of electronic transition causing the absorption, and it can take the values 1/2, 3/2, 2, and 3 for direct allowed, direct forbidden, indirect allowed, and indirect forbidden transitions, respectively [21]. The corresponding $(\alpha h\upsilon)^2$–$h\upsilon$ plots of the annealed In_2S_3 films were inserted in figure 2, from which we can deduce that the bandgaps were 2.80, 2.44, and 2.20 eV for the annealed IS1, IS2, and IS3 films, respectively, meaning that the films obtained under higher laser power have a smaller bandgap.

The energy bandgap of the polycrystalline semiconductor is known to be affected by the stoichiometric deviations, the variation of grain sizes [22], changes in preferred orientation of the films [23], dislocation density, and disorder at the grain boundaries [24]. No remarkable stoichiometric deviations or changes in preferred orientation have been observed in the XRD patterns or EDS spectra, so the surfaces of the films were further researched. Figure 3 shows the AFM micrographs of the annealed In_2S_3 films and the corresponding average surface roughness, grain size, and grain height. We can see that the average surface roughness of the IS1 film was 14.3 nm, which was remarkably decreased to 4.39 nm for the IS2 film and 0.91 nm for the IS3 film. Accordingly, the average height of the grains on the surface of the In_2S_3 films decreased from 308 to 5.36 nm. Since it is well known that the plasma 'plume' in the PLD system initiated by a higher laser power has much higher energy, the grains deposited on the substrate will keep moving to release the energy. Agglomeration and rearrangement of adjacent isolated grains will then occur during the movement process—that is, the grains with

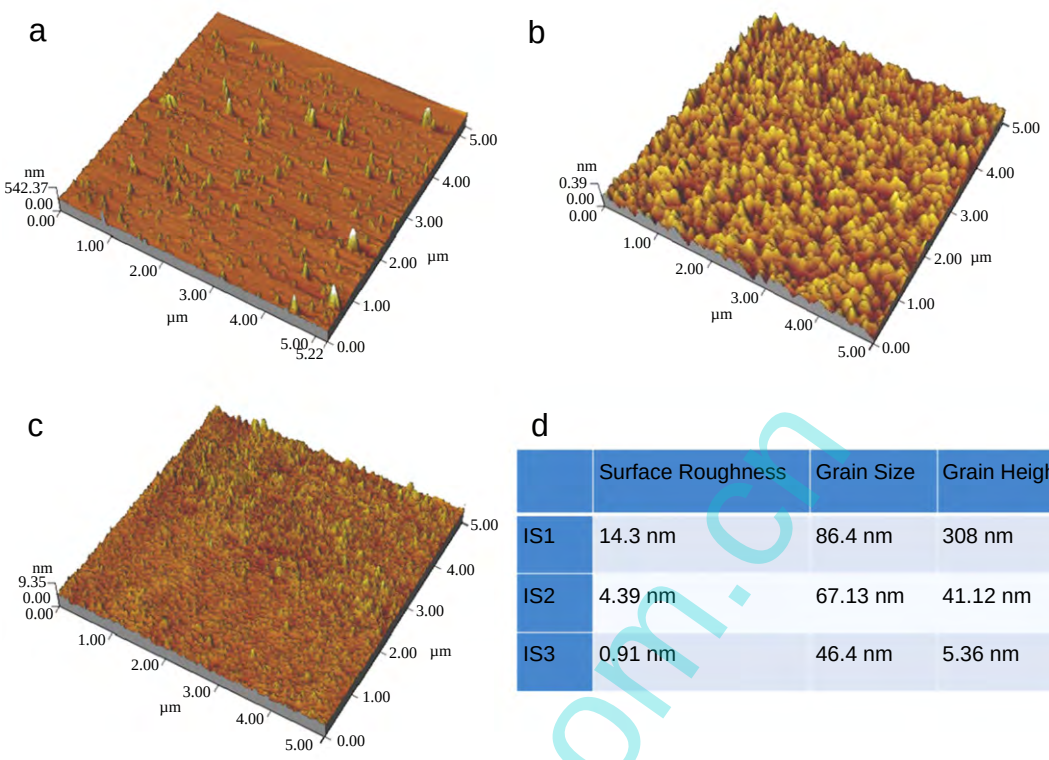

	Surface Roughness	Grain Size	Grain Height
IS1	14.3 nm	86.4 nm	308 nm
IS2	4.39 nm	67.13 nm	41.12 nm
IS3	0.91 nm	46.4 nm	5.36 nm

Figure 3. AFM micrographs of the annealed In_2S_3 films: (a) IS1, (b) IS2, and (c) IS3. (d) The average surface parameters of the annealed In_2S_3 films.

higher energy will keep growing after they are deposited. The grain growth can reduce the boundaries between the grains and the surface of each grain, resulting in a smoother surface with lower surface roughness and smaller grain height [25]. On the other hand, the average grain size of the films was found to decrease from 86.4 to 46.4 nm, which seemed inconsistent with the grain growth in the films caused by higher laser power. However, the average grain size given by AFM micrographs can only partially represent the size of the above-the-surface part of the grains. Based on the above discussion, we believe that as a result of further grain growth, the real grain size of the films increased with the increase in laser power, resulting in a decrease of the bandgap as shown in figure 2 [20].

Further electric and photoelectric characteristics of the In_2S_3 film were researched to investigate their potential application as the buffer layer in solar cells. Figure 4(a) shows the typical current density (J)–voltage (V) curves of both as-deposited and annealed IS3 films in the dark. The as-deposited IS3 film showed a high resistivity of about 380 Ω cm, which is comparable to the value of the 300 nm-thick thermal-deposited In_2S_3 films annealed at 300 °C [18]. However, the resistivity decreased to about 0.30 Ω cm after annealing, with a decrease of 3 orders of magnitude, meaning a dramatic improvement in conductivity. The transport properties of the annealed IS3 film are shown in figure 4(b). The J–V curves were measured under varied gate voltage, V_g, from −60 to +60 V, with a step of 40 V. Note that the conductance increased gradually with the increase of V_g, revealing the n-type nature of the annealed IS3 film.

Figure 4(c) shows the J–V curves of the heterojunction p^+-Si/annealed IS3 film. We can see clearly that the device exhibits a pronounced photovoltaic behavior upon light illumination with an open circuit voltage (V_{OC}) of 0.28 V and a short circuit current density (J_{SC}) of 7.85 μA cm^{-2}. The fill factor (FF) and power conversion efficiency (η) could be deduced to be 40.2% and ~0.04%, respectively, according to the following equations:

$$FF = \frac{J_m V_m}{J_{SC} V_{OC}} \quad (1)$$

$$\eta = \frac{J_m V_m}{SP_{in}} \quad (2)$$

where J_m and V_m are the current and voltage at the maximum power output, respectively. S is the effective heterojunction area (~0.86 cm^2) and P_{in} is the incident power density. The low η may be partially attributed to the white light we used in this study. The wavelength of the white light is centered at around

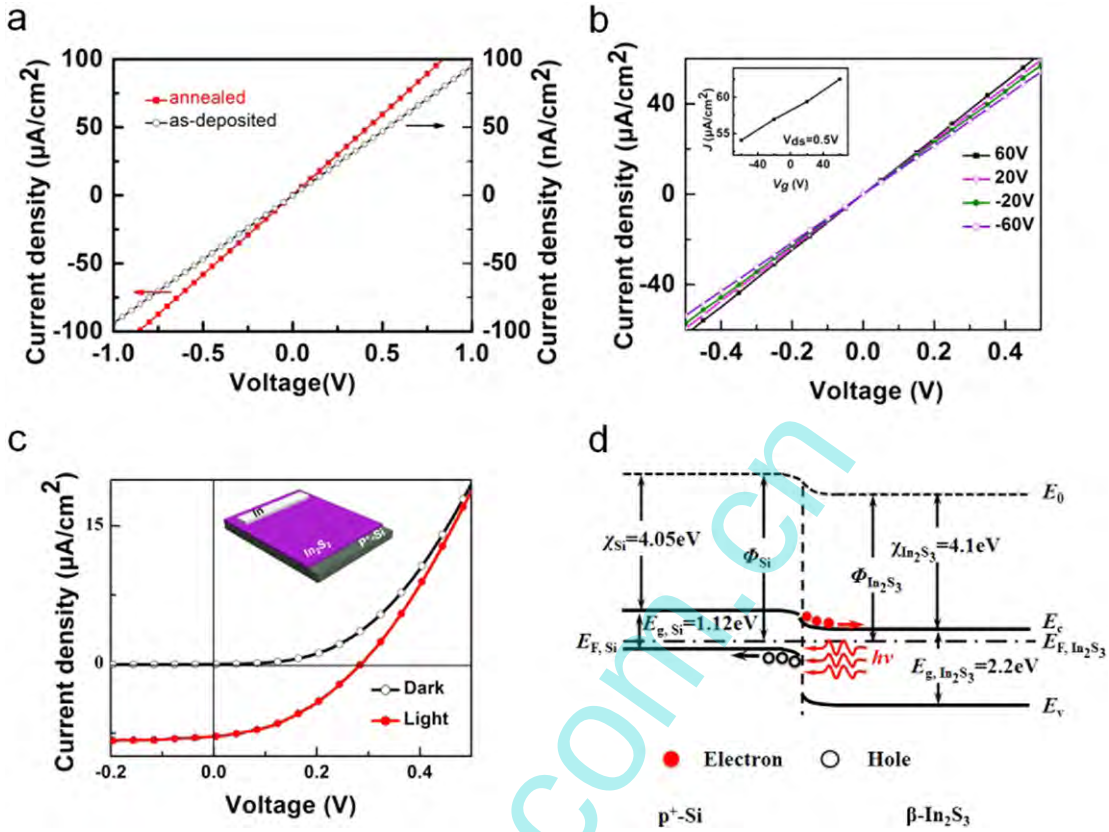

Figure 4. (a) The typical *J*–*V* curves of as-deposited and annealed IS3 film in the dark. (b) *J*–*V* curves measured with V_g increasing from −60 V to 60 V with a step of 40 V. The inset presents the corresponding *J*–V_g curve at $V = 0.5$ V. (c) *J*–*V* curves of the p^+-Si/annealed IS3 heterojunction in the dark and upon light illumination (white light, 2.6 mW cm^{-2}). The inset shows the schematic illustration of the device. (d) Energy band diagram of the p^+-Si/In_2S_3 heterojunction upon light illumination. Φ, χ, E_g., and E_F denote the work function, electron affinity, bandgap, and Fermi energy level of the corresponding materials marked in the subscripts, respectively. E_c, E_v, and E_0 are the conduction band minimum, valence band maximum, and vacuum energy level, respectively.

450 nm, which has been greatly absorbed by the In_2S_3 film but not by the absorption layer, resulting in a low η. Meanwhile, the large series resistance and the severe interface recombination of the junction may also be responsible for the small η. For the same reasons, although the bandgaps vary, no obvious difference has been observed between the photovoltaic behavior of the heterojunctions made from different In_2S_3 films, which are not shown here.

To elucidate the photovoltaic characteristics of the p^+-Si/In_2S_3 heterojunction, the energy band diagram of the device is illustrated in figure 4(d). A space-charge region is formed between p^+-Si and In_2S_3 when contacted. The built-in electric field is directed from In_2S_3 to p^+-Si. When the junction is illuminated by an incident light, electron-hole pairs will be excited by the photons with energy larger than the bandgap of Si. The photo-generated electron-hole pairs are then separated by the built-in electric field in opposite directions. The photo-generated electrons are diffused into In_2S_3, while the photo-generated holes are injected into p^+-Si, leading to a photocurrent.

4. Conclusions

In summary, stoichiometric tetragonal In_2S_3 films with the preferred orientation (103) were successfully deposited through the PLD method. The as-deposited In_2S_3 films were highly insulative and their conductivities were improved by 3 orders of magnitude after annealing in an N_2 atmosphere at 350 °C for 5 min. The bandgap of the annealed films decreased with an increase in the laser power used to deposit the films. The electric characteristics revealed the n-type conduction of the annealed films, and a remarkable photovoltaic behavior was observed on the heterojunction p^+-Si/annealed IS3 film, showing that the obtained In_2S_3 films may have great potential as the buffer layer in thin-film solar cells.

Acknowledgments

This work was supported by the National Natural Science Foundation of China (NSFC, Nos. 20901021, 21101051, 21301044, 61106010), the Natural Science Foundation of Anhui Province of China (No. 1408085MB31), and the Fundamental Research Funds for the Central Universities (Nos. 2013HGXJ0195, 2013HGCH0012, and 2014HGCH0013).

References

[1] Yu S H, Shu L, Wu Y S, Yang J, Xie Y and Qian Y T 1999 *J. Am. Ceram. Soc.* **82** 457
[2] Franzman M A and Brutchey R L 2009 *Chem. Mater.* **21** 1790
[3] Lokhande C D, Ennoui A, Patil P S, Giersig M, Diesner K, Muller M and Tributsch H 1999 *Thin Solid Films* **340** 18
[4] Jayakrishnan R H, John T T, Kartha C S, Vijayakumar K P, Jain D, Chandra L S S and Ganesan V J 2008 *J. Appl. Phys.* **103** 1
[5] Rengaraj S, Venkataraj S, Tai C W, Kim Y H, Repo E and Sillanpää M 2011 *Langmuir* **27** 5534
[6] Du W M, Zhu J, Li S X and Qian X F 2008 *Cryst. Growth. Des.* **8** 2130
[7] Tang J, Konstantatos G, Hinds S, Myrskog S, Pattantyus-Abraham A G, Clifford J and Sargent E H 2009 *ACS Nano* **3** 331
[8] Tang A W, Teng F, Wang Y, Hou Y B, Han W, Yi L X and Gao M Y 2008 *Nanoscale Res. Lett.* **3** 502
[9] Wilson K C, Sebastian T, John T T, Kartha C S, Vijayakumar K P, Magudapathi P and Nair K G M 2006 *Appl. Phys. Lett.* **89** 013510
[10] Sterner J, Malmstrom J and Stolt L 2005 *Prog. Photovolt., Res. Appl.* **13** 179
[11] Strohm A, Eisenmann L, Gebhardt R K, Harding A, Schlötzer T, Abou-Ras D and Schock H W 2005 *Thin Solid Films* **480** 162
[12] Kim W T and Kim C D 1986 *J. Appl. Phys.* **60** 2631
[13] Nomura R, Konishi K and Matsuda H 1991 *Thin Solid Films* **198** 339
[14] McCarthy R F, Weimer M S, Emery J D, Hock A S and Martinson A B F 2014 *ACS Appl. Mater. Interfaces* **6** 12137
[15] Pistor P, Caballero R, Hariskos D, Izquierdo-Roca V, Wächter R, Schorr S and Klenk R 2009 *Sol. Energy Mater. Sol. Cells* **93** 148
[16] Verma R, Datta D and Chirila A 2010 *J. Appl. Phys.* **108** 074904
[17] Nedyalkov N, Nikolov A, Atanasov P, Alexandrov M, Terakawa M and Shimizu H 2014 *Opt. Laser Technol.* **64** 41
[18] Pompilian O G, Dascalu G, Mihaila I, Gurlui S, Olivier M, Nemec P, Nazabal V, Cimpoesu N and Focsa C 2014 *Appl. Phys.* A **117** 197
[19] Late D J, Shaikh P A, Ruchita K, Kashid R V, Chaudhary M and Mahendra A 2014 *ACS Appl. Mater. Interfaces* **6** 15881
[20] Revathi N, Prathap P, Miles R W and Ramakrishna Reddy K T 2010 *Sol. Energy Mater. Sol. Cells* **94** 1487
[21] Qadri S B, Kim H, Horwitz J S and Chrisey D B 2000 *J. Appl. Phys.* **88** 6564
[22] Lokhande C D, Ubale A U and Patil P S 1997 *Thin Solid Films* **302** 1
[23] Mane R S and Lokhande C D 2003 *Mater. Chem. Phys.* **82** 347
[24] Dow J D and Redfield D 1972 *Phys. Rev.* B **5** 594
[25] Castanedo R, Jimenez O, Jimenez S, Marquez J, Mendoza A, Torres G and Maldonada A 1999 *J. Vac. Sci. Technol.* A **17** 1811